Computer Assisted Mechanics and Engineering Sciences, 15: 319–336, 2008.

Application of hybrid-Trefftz finite element method to frictional contact problems

Qing-Hua Qin
Department of Engineering, Australian National University
Canberra, ACT 0200, Australia

Ke-Yong Wang
School of Mechanical Engineering, Tianjin University, Tianjin, 300072, China

(Received in the final form November 5, 2008)

A contact algorithm, based on the hybrid-Trefftz (HT) finite element method (FEM), is developed for the solution of contact problems with Coulomb friction. Contact conditions are directly imposed with the aid of a direct constraint approach. On the other hand, static condensation technique is used to reduce the contact system to a smaller one which involves nodes within the potential contact surfaces only so that it may save computing time significantly. The final contact interface equation is constructed by considering contact conditions as additional equations. An incremental-iterative algorithm is introduced to determine proper load increments and find correct contact conditions. The applicability and accuracy of the proposed approach are demonstrated through three numerical problems.

1. Introduction

As an efficient and well-established numerical tool in computational mechanics, the HT finite element (FE) model has gained considerable attractions since its nascence [4] 30 years ago. This model, which is based on the idea of Trefftz method [25], assumes two groups of displacement fields independently. One, defined in the domain of the element, is often known as the intra-element field (or internal field, Trefftz field); the other, defined on the element boundary, is called the inter-element field (or frame field). In contrast to conventional FE or boundary element (BE) models, as highlighted in several reports [8, 18, 21], the HT FE model preserves the advantages of conventional FE and BE counterparts and discards some of their drawbacks. For example, in absence of body forces the HT FE formulation calls for integration along the element boundary only, as a consequence, it may be viewed as a special, symmetric, substructure-oriented boundary solution approach and thus possesses the advantages of conventional boundary element method (BEM); on the other hand, it also avoids the introduction of singular integral equations, appearing in BEM, which may be very laborious to build. So far the HT FE model has been successfully applied to plates [3, 13], Poisson's equation [7, 31], plane elasticity [6, 12], elastodynamic problems [2, 16], transient heat conduction [5], geometrically nonlinear plates [14, 15, 17, 23], materially nonlinear elasticity [22, 30], etc. Recently, Wang *et al.* [26] developed an algorithm for analyzing elastic contact problems without friction. This paper is an extension of our previous work [26] to include friction effect. The structure of this paper is arranged as follows. The HT FE theory is concisely reviewed for the completeness. Subsequently, the corresponding numerical implementation for the HT FE formulations is derived. In the contact analysis static condensation technique [27] is used to reduce the considered system down to a smaller one so that much more computational efforts may be remarkably saved. In addition, contact conditions, namely compatibility of displacements and equilibrium of tractions on the interface are directly imposed with the aid of a direct constraint approach [11]. An automatic

incremental-iterative algorithm has been employed to determine the load increments and find the correct contact conditions. The performance of the proposed procedure is assessed though three classical examples. The obtained results show a good agreement with those from commercial FE software ABAQUS.

2. Theory

2.1. Assumed fields

The governing differential equations for the linear response of an elastic body with domain Ω and boundary Γ, may be summarized as follows,

$$\mathbf{L}\boldsymbol{\sigma} + \bar{\mathbf{b}} = \mathbf{0}, \qquad \boldsymbol{\sigma} = \mathbf{D}\boldsymbol{\varepsilon}, \qquad \boldsymbol{\varepsilon} = \mathbf{L}^T\mathbf{u}, \qquad \text{in } \Omega \tag{1a–c}$$

together with

$$\mathbf{u} = \bar{\mathbf{u}} \qquad \text{on } \Gamma_u\,, \tag{1d}$$

$$\mathbf{t} = \mathbf{A}\boldsymbol{\sigma} = \bar{\mathbf{t}} \qquad \text{on } \Gamma_t\,. \tag{1e}$$

In the HT FE form, Eqs. (1a–e) should be completed by the following inter-element continuity requirements,

$$\mathbf{u}_a = \mathbf{u}_b \qquad \text{on } \Gamma_a \cap \Gamma_b\,, \text{ (conformity)}, \tag{1f}$$

$$\mathbf{t}_a = \mathbf{t}_b \qquad \text{on } \Gamma_a \cap \Gamma_b\,, \text{ (traction reciprocity)}, \tag{1g}$$

where $\mathbf{u}$, $\boldsymbol{\varepsilon}$, $\boldsymbol{\sigma}$, $\mathbf{t}$ and $\bar{\mathbf{b}}$ are displacements, strains, stresses, boundary tractions and body forces, respectively, $\bar{\mathbf{u}}$ and $\bar{\mathbf{t}}$ designate prescribed values, and $\mathbf{D}$, $\mathbf{L}$, $\mathbf{A}$ are given as

$$\mathbf{L} = \begin{bmatrix} \frac{\partial}{\partial x} & 0 & \frac{\partial}{\partial y} \\ 0 & \frac{\partial}{\partial y} & \frac{\partial}{\partial x} \end{bmatrix}^T, \quad \mathbf{D} = \frac{E^*}{1-\nu^{*2}} \begin{bmatrix} 1 & \nu^* & 0 \\ \nu^* & 1 & 0 \\ 0 & 0 & \frac{1-\nu^*}{2} \end{bmatrix}, \quad \mathbf{A} = \begin{bmatrix} n_x & 0 & n_y \\ 0 & n_y & n_x \end{bmatrix}, \tag{2a–c}$$

where $E^* = E$, $\nu^* = \nu$ for plane stress analysis and $E^* = E/(1-\nu^2)$, $\nu^* = \nu/(1-\nu)$ for plane strain analysis. Here, E and ν are Young's modulus and Poisson's ratio, respectively, $n_x = \cos\alpha$, $n_y = \sin\alpha$, and α is direction angle of the outward normal at a given point on the element boundary as shown in Fig. 1, Γ_u and Γ_t are the boundaries on which prescribed displacements and surface tractions are imposed.

To perform the HT FE analysis, the whole domain Ω is divided into a number of subdomains Ω_e (see Fig. 1). For each Ω_e, two groups of independent fields are assumed in the following way [6]:

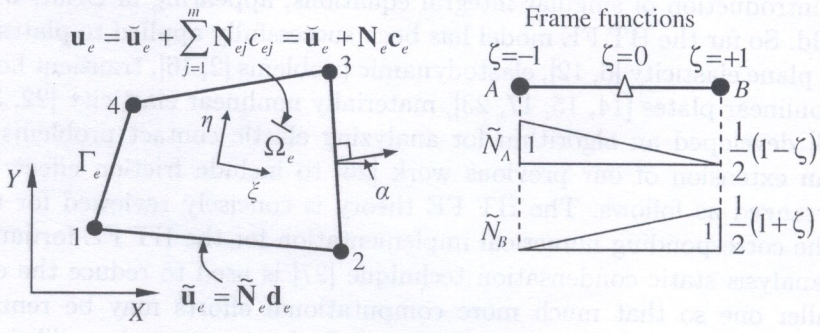

Fig. 1. Typical four-node HT element together with its frame functions

1. The non-conforming Trefftz field is expressed by

$$\mathbf{u}_e = \breve{\mathbf{u}}_e + \sum_{j=1}^{m} \mathbf{N}_{ej} c_{ej} = \breve{\mathbf{u}}_e + \mathbf{N}_e \mathbf{c}_e \qquad \text{in } \Omega_e \tag{3}$$

where $\breve{\mathbf{u}}_e$ and $\mathbf{N}_e$ are, respectively, the particular and homogeneous solutions (Trefftz functions) to Eq. (1a), $\mathbf{c}_e$ stands for unknown parameters, and m represents the number of homogeneous solutions (Trefftz terms). In plane elasticity, a complete set of homogeneous solutions $\mathbf{N}_e$ can be generated in a systematic way from Muskhelishvili's complex variable formulation [6] and is presented in Appendix A for reference.

2. An auxiliary conforming frame field

$$\tilde{\mathbf{u}}_e = \tilde{\mathbf{N}}_e \mathbf{d}_e \qquad \text{on } \Gamma_e \tag{4}$$

is independently assumed along the element boundary in terms of nodal DOF $\mathbf{d}_e$, where $\tilde{\mathbf{N}}_e$ designates the frame functions, namely the conventional FE interpolating functions. Such field is required to conform across the inter-element boundary.

2.2. Element analysis and numerical implementation

Based on the modified principle given in [19, 20] one can derive the HT FE formulation for plane elastic problems. The correlative functional is given as

$$\Pi_m = \sum_e \Pi_{me} = \sum_e \left[\iint_{\Omega_e} \frac{1}{2} \boldsymbol{\sigma}_e^T \mathbf{C} \boldsymbol{\sigma}_e \, \mathrm{d}\Omega - \int_{\Gamma_{eu}} \mathbf{t}_e \bar{\mathbf{u}}_e \, \mathrm{d}\Gamma - \int_{\Gamma_{et}} (\mathbf{t}_e - \bar{\mathbf{t}}_e) \, \tilde{\mathbf{u}}_e \, \mathrm{d}\Gamma - \int_{\Gamma_{eI}} \mathbf{t}_e \tilde{\mathbf{u}}_e \, \mathrm{d}\Gamma \right] \tag{5}$$

where $\mathbf{C} = \mathbf{D}^{-1}$, $\Gamma_e = \Gamma_{eu} \cup \Gamma_{et} \cup \Gamma_{eI}$, $\Gamma_{eu} = \Gamma_u \cap \Gamma_e$, $\Gamma_{et} = \Gamma_t \cap \Gamma_e$, Γ_{eI} is the inter-element boundary, $\boldsymbol{\sigma}_e$, $\mathbf{t}_e$ stand for the element stress and boundary traction fields respectively such that

$$\boldsymbol{\sigma}_e = \breve{\boldsymbol{\sigma}}_e + \sum_{j=1}^{m} \mathbf{T}_{ej} c_j = \breve{\boldsymbol{\sigma}}_e + \mathbf{T}_e \mathbf{c}_e \,, \tag{6}$$

$$\mathbf{t}_e = \breve{\mathbf{t}}_e + \sum_{j=1}^{m} \mathbf{Q}_{ej} c_j = \breve{\mathbf{t}}_e + \mathbf{Q}_e \mathbf{c}_e \,, \tag{7}$$

where $\breve{\boldsymbol{\sigma}}_e$, $\breve{\mathbf{t}}_e$ and $\mathbf{T}_e$, $\mathbf{Q}_e$ are, respectively, the resulting stress and boundary traction particular and homogeneous solutions pertinent to $\breve{\mathbf{u}}_e$ and $\mathbf{N}_e$. The detailed expressions of $\breve{\mathbf{u}}_e$, $\breve{\boldsymbol{\sigma}}_e$, $\breve{\mathbf{t}}_e$, $\mathbf{N}_e$, $\mathbf{T}_e$, $\mathbf{Q}_e$ are listed in Appendix A.

Substituting Eqs. (4), (6) and (7) into the functional (5) and applying stationary condition with respect to $\mathbf{c}_e$ and $\mathbf{d}_e$, one may obtain the customary force-displacement relationship, namely the HT element stiffness matrix

$$\mathbf{K}_e \mathbf{d}_e = \mathbf{P}_e \tag{8}$$

where

$$\mathbf{K}_e = \mathbf{G}_e^T \mathbf{H}_e^{-1} \mathbf{G}_e \,, \qquad \mathbf{P}_e = \mathbf{G}_e^T \mathbf{H}_e \mathbf{g}_e + \mathbf{h}_e \,, \tag{9a,b}$$

are, respectively, the HT element stiffness matrix and equivalent nodal force vector. And the involved matrices $\mathbf{H}_e$ (the so-called element flexibility matrix), $\mathbf{G}_e$, $\mathbf{h}_e$ and $\mathbf{g}_e$ are explicitly expressed as

$$\mathbf{H}_e = \int_{\Gamma_e} \mathbf{Q}_e^T \mathbf{N}_e \, \mathrm{d}\Gamma = \int_{\Gamma_e} \mathbf{N}_e^T \mathbf{Q}_e \, \mathrm{d}\Gamma, \tag{10a}$$

$$\mathbf{G}_e = \int_{\Gamma_{et}+\Gamma_{eI}} \mathbf{Q}_e^T \tilde{\mathbf{N}}_e \, \mathrm{d}\Gamma, \tag{10b}$$

$$\mathbf{h}_e = -\frac{1}{2} \int_{\Omega_e} \mathbf{N}_e^T \bar{\mathbf{b}}_e \, \mathrm{d}\Omega - \frac{1}{2} \int_{\Gamma_e} (\mathbf{Q}_e^T \breve{\mathbf{u}}_e + \mathbf{N}_e^T \breve{\mathbf{t}}_e) \, \mathrm{d}\Gamma + \int_{\Gamma_{eu}} \mathbf{Q}_e^T \bar{\mathbf{u}}_e \, \mathrm{d}\Gamma, \tag{10c}$$

$$\mathbf{g}_e = \int_{\Gamma_{et}} \tilde{\mathbf{N}}_e^T (\bar{\mathbf{t}}_e - \breve{\mathbf{t}}_e) \, \mathrm{d}\Gamma - \int_{\Gamma_{eI}} \tilde{\mathbf{N}}_e^T \breve{\mathbf{t}}_e \, \mathrm{d}\Gamma. \tag{10d}$$

In numerical implementation of the HT FE model, a dimensionless coordinate system

$$\begin{cases} \xi = x/a \\ \eta = y/a \end{cases} \tag{11}$$

has to be used to ensure a good numerical conditioning of the element flexibility matrix $\mathbf{H}_e$ and prevent overflow, where x, y are local Cartesian coordinates, a stands for the average distance between the element nodes and its centroid (the element characteristic length), their expressions read

$$x = X - X_o = X - \frac{1}{n} \sum_{i=1}^{n} X_i \,, \tag{12a}$$

$$y = Y - Y_o = Y - \frac{1}{n} \sum_{i=1}^{n} Y_i \,, \tag{12b}$$

$$a = \frac{1}{n} \sum_{i=1}^{n} \sqrt{x_i^2 + y_i^2} \,, \tag{12c}$$

and in which X, Y are the global Cartesian coordinates, n stands for the number of nodes on an element.

It should be noted that the previously defined matrices and vectors associated with the element are constructed in the local Cartesian coordinate system (x, y). Now, let us transform them into the dimensionless coordinate system (ξ, η), the matrices involved in $\mathbf{K}_e$ may be rewritten as

$$\mathbf{N}_e = \mathbf{N}_e(x, y) = \mathbf{N}_e(\xi, \eta) \, \mathbf{\Phi}, \tag{13a}$$

$$\mathbf{Q}_e = \mathbf{Q}_e(x, y) = \frac{1}{a} \mathbf{Q}_e(\xi, \eta) \, \mathbf{\Phi}, \tag{13b}$$

$$\tilde{\mathbf{N}}_e = \tilde{\mathbf{N}}_e(x, y) = \tilde{\mathbf{N}}_e(\xi, \eta), \tag{13c}$$

$$\bar{\mathbf{b}}_e = \bar{\mathbf{b}}_e(x, y) = \bar{\mathbf{b}}_e(\xi, \eta), \tag{13d}$$

$$\bar{\mathbf{u}}_e = \bar{\mathbf{u}}_e(x, y) = \bar{\mathbf{u}}_e(\xi, \eta), \tag{13e}$$

$$\bar{\mathbf{t}}_e = \bar{\mathbf{t}}_e(x, y) = \bar{\mathbf{t}}_e(\xi, \eta), \tag{13f}$$

$$\breve{\mathbf{u}}_e = \breve{\mathbf{u}}_e(x, y) = a^2 \, \breve{\mathbf{u}}_e(\xi, \eta), \tag{13g}$$

$$\breve{\mathbf{t}}_e = \breve{\mathbf{t}}_e(x, y) = a \, \breve{\mathbf{t}}_e(\xi, \eta), \tag{13h}$$

where $\mathbf{\Phi} = \mathrm{diag}\,(\, a \;\; a \;\; a \;\; a^2 \;\; a^2 \;\; a^2 \;\; a^2 \;\; a^3 \;\; a^3 \;\; \cdots\,)$ may be called the element characteristic diagonal matrix. Substituting relations (13a,b) and $\mathrm{d}\Gamma = a \, \mathrm{d}s$ into Eq. (10a), one can obtain

$$\begin{aligned} \mathbf{H}_e = \mathbf{H}_e(x, y) &= \int_{\Gamma_e} \mathbf{Q}_e^T(x, y) \, \mathbf{N}_e(x, y) \, \mathrm{d}\Gamma = \int_{\Gamma_e} \mathbf{\Phi}^T \mathbf{Q}_e^T(\xi, \eta) \, \mathbf{N}_e(\xi, \eta) \, \mathrm{d}s \\ &= \mathbf{\Phi}^T \mathbf{H}_e(\xi, \eta) \, \mathbf{\Phi} = \mathbf{\Phi} \, \mathbf{H}_e(\xi, \eta) \, \mathbf{\Phi}. \end{aligned} \tag{14a}$$

Analogously,

$$\mathbf{H}_e^{-1} = \mathbf{H}_e^{-1}(x,y) = \mathbf{\Phi}^{-1}\,\mathbf{H}_e^{-1}(\xi,\eta)\,\mathbf{\Phi}^{-T} = \mathbf{\Phi}^{-1}\,\mathbf{H}_e^{-1}(\xi,\eta)\,\mathbf{\Phi}^{-1}, \tag{14b}$$

$$\mathbf{G}_e = \mathbf{G}_e(x,y) = \mathbf{\Phi}^T\mathbf{G}_e(\xi,\eta) = \mathbf{\Phi}\,\mathbf{G}_e(\xi,\eta) \tag{14c}$$

$$\mathbf{h}_e = \mathbf{h}_e(x,y) = \mathbf{\Phi}^T\mathbf{h}_e(\xi,\eta) = \mathbf{\Phi}\,\mathbf{h}_e(\xi,\eta) \tag{14d}$$

$$\mathbf{g}_e = \mathbf{g}_e(x,y) = \mathbf{g}_e(\xi,\eta) \tag{14e}$$

Then, Eqs. (9a,b) can be rewritten as

$$\mathbf{K}_e = \mathbf{K}_e(x,y) = \mathbf{K}_e(\xi,\eta), \qquad \mathbf{P}_e = \mathbf{P}_e(x,y) = \mathbf{P}_e(\xi,\eta), \tag{15a,b}$$

by substitution of Eqs. (14a–e). It is obvious that $\mathbf{K}_e$ and $\mathbf{P}_e$ remain unchanged not only in form and but also in magnitude from the local Cartesian coordinate system to the dimensionless coordinate system. In practice one can, therefore, replace x and y by ξ and η directly to evaluate the HT element stiffness equation.

3. Application to contact problems

3.1. Contact conditions

Consider a two-body contact system which occupies domains Ω^1 and Ω^2 (Fig. 2). The parts Γ_c^1 and Γ_c^2 of their respective boundaries Γ^1 and Γ^2 qualify as potential contact surfaces which should be chosen to be sufficiently large to contain actual contact interface Γ_c ($\Gamma_c^1 \cap \Gamma_c^2$). It is observed that the boundaries Γ^β of individual body consist of three disjoint parts Γ_u^β, Γ_t^β and Γ_c^β, where $\beta = 1, 2$, and Γ_u^β, Γ_t^β are the parts where displacements and tractions are prescribed.

The discrete points on both potential contact surfaces should match so that the contact behavior occurs just between each pair of opposite nodes $(i^1 - i^2)$ as shown in Fig. 3. A contact coordinate system as shown in Fig. 3 is defined in the undeformed configuration. Obviously, the approximate common unit normal at node-pair $(i^1 - i^2)$ may be taken as [10, 28]

$$\mathbf{n}_i = \frac{\mathbf{n}_i^2 - \mathbf{n}_i^1}{\|\mathbf{n}_i^2 - \mathbf{n}_i^1\|} = [-\sin\phi_i\,,\ \cos\phi_i]\,. \tag{16}$$

Rotating $\mathbf{n}_i$ anticlockwise by 90° , one can obtain the corresponding tangential direction $\boldsymbol{\tau}_i$ as shown in Fig. 3, in which φ_i designates the angle between $\boldsymbol{\tau}_i$ and X axis.

The contact conditions can be determined by considering compatibility of displacements and equilibrium of tractions on the contact surfaces consist of four statuses (open, stick, forward sliding and backward sliding). Coulomb frictional law, represented in Fig. 4, was used in this work. With

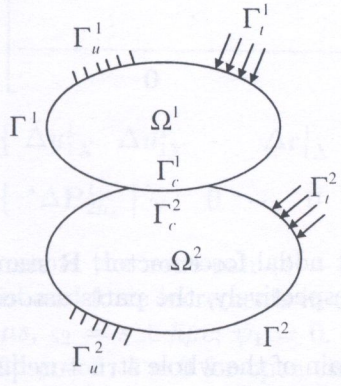

Fig. 2. Schematic representation of contact problem

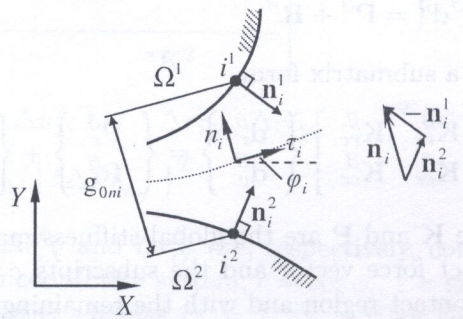

Fig. 3. Contact coordinate system

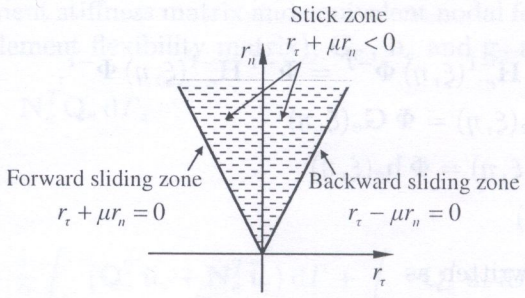

Fig. 4. Coulomb friction law and sub-zone of contact

Table 1. Incremental solution conditions for various statuses

Contact statuses	Incremental solution conditions	
Open	$\Delta r_{in}^1 + \Delta r_{in}^2 = 0$ $\Delta r_{in}^1 = 0$	$\Delta r_{i\tau}^1 + \Delta r_{i\tau}^2 = 0$ $\Delta r_{i\tau}^1 = 0$
Stick	$\Delta r_{in}^1 + \Delta r_{in}^2 = 0$ $\Delta u_{in}^1 - \Delta u_{in}^2 = g_{in}^s$	$\Delta r_{i\tau}^1 + \Delta r_{i\tau}^2 = 0$ $\Delta u_{i\tau}^1 - \Delta u_{i\tau}^2 = 0$
Forward sliding	$\Delta r_{in}^1 + \Delta r_{in}^2 = 0$ $\Delta u_{in}^1 - \Delta u_{in}^2 = g_{in}^s$	$\Delta r_{i\tau}^1 + \Delta r_{i\tau}^2 = 0$ $\Delta r_{i\tau}^1 + \mu \Delta r_{in}^1 = 0$
Inverse sliding	$\Delta r_{in}^1 + \Delta r_{in}^2 = 0$ $\Delta u_{in}^1 - \Delta u_{in}^2 = g_{in}^s$	$\Delta r_{i\tau}^1 + \Delta r_{i\tau}^2 = 0$ $\Delta r_{i\tau}^1 - \mu \Delta r_{in}^1 = 0$

the Coulomb frictional law the tangential component of the contact forces, or frictional force, can be exerted without slip (under stick status) until a certain threshold is overcome to allow sliding. The threshold is proportional to the magnitude of the normal contact forces as well as friction coefficient μ. In Fig. 4, stick zone, forward and backward sliding zones are, more especially, subdivided graphically. Table 1 demonstrates all the incremental contact conditions for each status of the node-pair $(i^1 - i^2)$. In which Δu_{in}^β and $\Delta u_{i\tau}^\beta$ designate the normal and tangential displacement increments on the potential contact surfaces whereas Δr_{in}^β and $\Delta r_{i\tau}^\beta$ denote the normal and tangential force increments, g_{in}^s is the normal gap at beginning of the sth load step.

3.2. Incremental contact interface equation

A set of equations can be established by assembling Eq. (8) over all the elements according to the standard assembly procedure. Doing so separately for each of the contacting bodies the resulting sets of equations may be formulated respectively as

$$\mathbf{K}^\beta \mathbf{d}^\beta = \mathbf{P}^\beta + \mathbf{R}^\beta \tag{17a}$$

or in a submatrix form

$$\begin{bmatrix} \mathbf{K}_{rr}^\beta & \mathbf{K}_{rc}^\beta \\ \mathbf{K}_{cr}^\beta & \mathbf{K}_{cc}^\beta \end{bmatrix} \begin{Bmatrix} \mathbf{d}_r^\beta \\ \mathbf{d}_c^\beta \end{Bmatrix} = \begin{Bmatrix} \mathbf{P}_r^\beta \\ \mathbf{P}_c^\beta \end{Bmatrix} + \begin{Bmatrix} \mathbf{0} \\ \mathbf{R}_c^\beta \end{Bmatrix}, \tag{17b}$$

where $\mathbf{K}$ and $\mathbf{P}$ are the global stiffness matrix and equivalent nodal force vector, $\mathbf{R}$ stands for the contact force vector and the subscripts c and r designate, respectively, the parts associated with the contact region and with the remaining region.

Generally, the contact region is small compared to the domain of the whole structure [24]. Therefore, one can use static condensation [27] to reduce each of the bodies to including the individual potential contact surface of each contact body. This may save computing time significantly. Then

introducing the prescribed displacement condition (1d) into (17a,b) and performing the Gaussian elimination process yields a reduced system of equations

$$ {}^{*}\mathbf{K}^{\beta}\mathbf{d}_c^{\beta} - \mathbf{R}_c^{\beta} = {}^{*}\mathbf{P}^{\beta} \tag{18} $$

where

$$ {}^{*}\mathbf{K}^{\beta} = \mathbf{K}_{cc}^{\beta} - \mathbf{K}_{cr}^{\beta}\mathbf{K}_{rr}^{\beta\ -1}\mathbf{K}_{cr}^{\beta\ T}, \tag{19a} $$

$$ {}^{*}\mathbf{P}^{\beta} = \mathbf{P}_c^{\beta} - \mathbf{K}_{cr}^{\beta}\mathbf{K}_{rr}^{\beta\ -1}\mathbf{P}_r^{\beta}. \tag{19b} $$

Here ${}^{*}\mathbf{K}^{\beta}$ is a $2n_c \times 2n_c$ matrix and ${}^{*}\mathbf{P}^{\beta}$ is a $2n_c$ vector and both of them are obtained simultaneously at an intermediate step of the Gaussian elimination process, and in which n_c is the number of candidate node-pairs.

To solve Eq. (18) for $\mathbf{d}_c^{\beta}$, it is necessary to use contact conditions defined on the interface. For convenience, the contact conditions for each node-pair as shown in Table 1 are transformed into the global Cartesian coordinate system using the following transformation matrix,

$$ \mathbf{\Psi}_i = \begin{bmatrix} \cos\phi_i & \sin\phi_i \\ -\sin\phi_i & \cos\phi_i \end{bmatrix}. \tag{20} $$

The final system, namely the contact interface equation, may be synthesized in the incremental form

$$ \mathbf{\Xi}\,\Delta\mathbf{X} = \Delta\mathbf{\Theta} \tag{21} $$

where

$$ \mathbf{\Xi} = \begin{array}{c} \begin{array}{cccccccccccc} \overset{2i-1}{\downarrow} & & \overset{2i}{\downarrow} & & \overset{2n_c+2i-1}{\downarrow} & & \overset{2n_c+2i}{\downarrow} & & \overset{4n_c+2i-1}{\downarrow} & & \overset{4n_c+2i}{\downarrow} & \overset{6n_c+2i-1}{\downarrow} \quad \overset{6n_c+2i}{\downarrow} \end{array} \\ \left[\begin{array}{cccccccccccc} \multicolumn{2}{c}{{}^{*}\mathbf{K}^1} & & \multicolumn{2}{c}{\mathbf{I}} & & \multicolumn{2}{c}{\mathbf{0}} & & \multicolumn{2}{c}{\mathbf{0}} & \\ \hline \vdots & \vdots & & \vdots & \vdots & & \vdots & \vdots & & \vdots & \vdots & \\ \cdots\ 0 & 0 & \cdots & -s & c & \cdots & 0 & 0 & \cdots & -s & c & \cdots \\ \vdots & \vdots & & \vdots & \vdots & & \vdots & \vdots & & \vdots & \vdots & \\ \cdots\ 0 & 0 & \cdots & c & s & \cdots & 0 & 0 & \cdots & c & s & \cdots \\ \vdots & \vdots & & \vdots & \vdots & & \vdots & \vdots & & \vdots & \vdots & \\ \cdots\ \hbar s & -\hbar c & \cdots & -\wp s & -\wp c & \cdots & -\hbar s & \hbar c & \cdots & 0 & 0 & \cdots \\ \vdots & \vdots & & \vdots & \vdots & & \vdots & \vdots & & \vdots & \vdots & \\ \cdots\ \hbar\psi_2 c & \hbar\psi_2 s & \cdots & \psi_1\varsigma_1 & \psi_1\varsigma_2 & \cdots & \hbar\psi_2 c & \hbar\psi_2 s & \cdots & 0 & 0 & \cdots \\ \vdots & \vdots & & \vdots & \vdots & & \vdots & \vdots & & \vdots & \vdots & \\ \hline \multicolumn{2}{c}{\mathbf{0}} & & \multicolumn{2}{c}{\mathbf{0}} & & \multicolumn{2}{c}{\mathbf{I}} & & \multicolumn{2}{c}{{}^{*}\mathbf{K}^2} & \end{array}\right] \end{array} \begin{array}{l} \\ \\ \leftarrow 2n_c+i \\ \\ \leftarrow 3n_c+i \\ \\ \leftarrow 4n_c+i \\ \\ \leftarrow 5n_c+i \\ \\ \end{array} \quad \left.\begin{array}{l} \\ \\ \\ \\ \\ \\ \\ \\ \end{array}\right\} \text{contact conditions} \tag{22} $$

$$ \Delta\mathbf{X} = \left\{ \Delta u_{1X}^1 \ \ \Delta u_{1Y}^1 \ \cdots\ \Delta r_{1X}^1 \ \ \Delta r_{1Y}^1 \ \cdots\ \Delta u_{1X}^2 \ \ \Delta u_{1Y}^2 \ \cdots\ \Delta r_{1X}^2 \ \ \Delta r_{1Y}^2 \ \cdots \right\}^T \tag{23} $$

$$ \Delta\mathbf{\Theta} = \left\{ {}^{*}\Delta\mathbf{P}_{2n_c}^1 \,\middle|\, \cdots\ 0\ \cdots\ 0\ \cdots\ g_{in}^b\ \cdots\ 0\ \cdots \,\middle|\, {}^{*}\Delta\mathbf{P}_{2n_c}^2 \right\}^T \tag{24} $$

Here i represents the node-pair $(i^1 - i^2)$; Δu_{iX}^{β}, Δu_{iY}^{β}, Δr_{iX}^{β} and Δr_{iY}^{β} are, respectively, contact displacement and force increments in the global Cartesian coordinate system; $c = \cos\phi_i$, $s = \sin\phi_i$, $\varsigma_1 = c \mp \hbar\mu s$, $\varsigma_2 = s \pm \hbar\mu c$; $\psi_1 = 0$, $\psi_2 = 1$ for stick status whereas $\psi_1 = 1$, $\psi_2 = 0$ for sliding statuses; and $\wp = 1$, $\hbar = 0$ for open status whereas $\wp = 0$, $\hbar = 1$ for contact.

Using the contact interface formulation presented previously, a HT FE program has been written in FORTRAN. The corresponding flow chart is shown in Fig. 5. In this figure there exist two loops

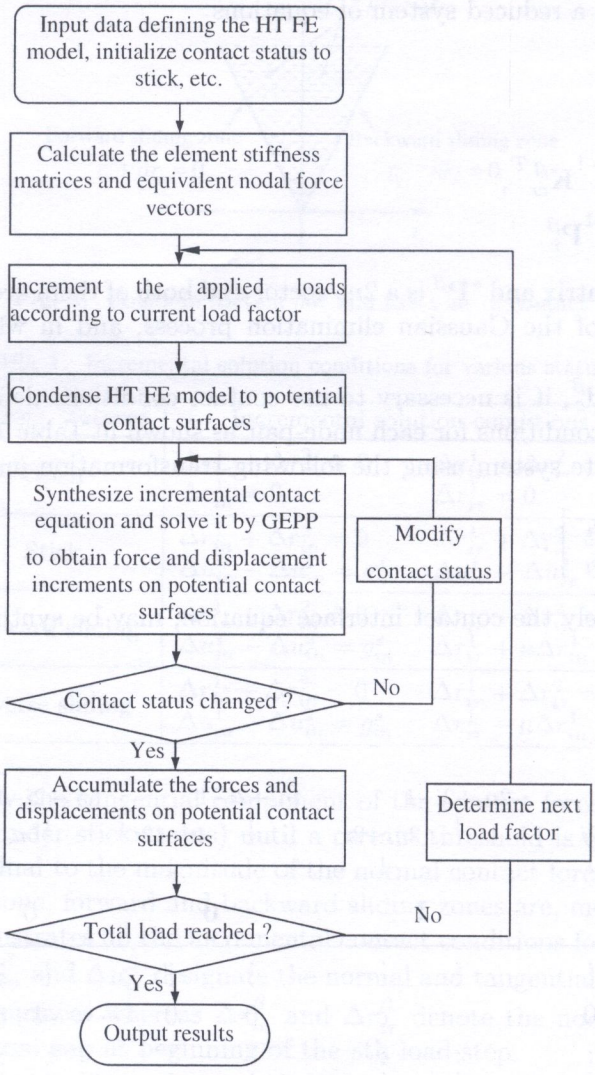

Fig. 5. Flow chart of incremental HT FE procedure for contact analysis

Table 2. Iterative criterion for contact conditions

Previous iteration	Future iteration			
	Open	Stick	Forward sliding	Inverse sliding
Open	$\Delta l_{in} > 0$	$\Delta l_{in} \le 0$ $\lvert\Delta l_{i\tau}\rvert \le -\mu\Delta l_{in}$	$\Delta l_{in} \le 0$ $\Delta l_{i\tau} > -\mu\Delta l_{in}$	$\Delta l_{in} \le 0$ $\Delta l_{i\tau} < \mu\Delta l_{in}$
Stick	$r_{in} \le 0$	$r_{in} > 0$ $\lvert r_{i\tau}\rvert < \mu r_{in}$	$r_{in} > 0$ $r_{i\tau} \le -\mu r_{in}$	$r_{in} > 0$ $r_{i\tau} \ge \mu r_{in}$
Forward sliding	$r_{in} \le 0$	$r_{in} > 0$ $-2\mu r_{in} \le \Delta l_{i\tau} \le 0$	$r_{in} > 0$ $\Delta l_{i\tau} > 0$	$r_{in} > 0$ $\Delta l_{i\tau} < -2\mu r_{in}$
Inverse sliding	$r_{in} \le 0$	$r_{in} > 0$ $2\mu r_{in} \ge \Delta l_{i\tau} \ge 0$	$r_{in} > 0$ $\Delta l_{i\tau} > 2\mu r_{in}$	$r_{in} > 0$ $\Delta l_{i\tau} < 0$

where $\Delta l_{in} = \Delta u^1_{in} - \Delta u^2_{in}$, $\Delta l_{i\tau} = \Delta u^1_{i\tau} - \Delta u^2_{i\tau}$, $r_{in} = r^1_{in}$, $r_{i\tau} = r^1_{in}$.

where the outer loop is used to determine the load increment while the inner loop to trigger iteration according to the criterion [1] given in Table 2. Due to the fact that zero appears on the diagonal of Ξ in Eq. (21), the solution process was carried on using Gaussian elimination with partial pivoting (GEPP) [29].

The procedure in determining load increment follows that of [28] and we will omit it here. The basic idea is that within each increment just one node-pair comes into contact and iterations are performed over all the current contacting node-pairs until convergence is achieved. Therefore, the vector $\mathbf{X}$ containing accumulated contact forces and associated displacements after s increments is updated as

$$\mathbf{X}^s = \mathbf{X}^{s-1} + \Delta\mathbf{X}^{s-1}. \tag{25}$$

After the total load is applied, the final contact forces and associated displacements are achieved. Then the normal and tangential contact stresses σ_{in}, $\sigma_{i\tau}$ of the node-pair i may be written as

$$\sigma_{in} = r_{in}^1/S_i\,, \qquad \sigma_{i\tau} = r_{i\tau}^1/S_i\,, \tag{26}$$

and the tangential relative slip $s_i$are given by

$$s_i = u_{i\tau}^1 - u_{i\tau}^2\,, \tag{27}$$

where S_i stands for the sub-area controlled by node-pair i.

4. Numerical assessments

To illustrate the performance of the procedure developed in this paper, there examples of a punch indented on a foundation, a cylinder on a rigid half-space, and a layer pressed on a substrate are considered. In all the three examples, only the right half of the solution domain is modeled using four-node HT elements due to the symmetry of the problems. The plane strain condition is assumed in the analysis. Results obtained from HT FEM are compared with ABAQUS 6.2 whose normal and tangential contact behaviors are respectively selected to "hard" contact and Lagrange multiplier and element type is set to 4-node bilinear plane strain quadrilateral, hybrid, constant (CPE4H).

4.1. A punch indented on a foundation

The geometry, properties, loads and boundary conditions shown in Fig. 6a are considered in this example [26]. Because of the symmetry of the problem, only the right half of the system is modeled by an element mesh, as illustrated in Fig. 6b. It should be mentioned that the proper choice of the number m of Trefftz terms is of great significance to the element performance and to the stability of the solution [9]. In order to find the optimal number of Trefftz terms, a range of m as shown in Table 3 according to the limited conditions (A7) and (A8) of Appendix A are chosen. Then, a test is carried out on a punch indented on a foundation depicted in Fig. 6a. The identical elastic properties for the two bodies are selected such that $E^1 = E^2 = 4000\,\text{MPa}$ and $\nu^1 = \nu^2 = 0.35$. The uniform pressure of $q = 1.2\,\text{MPa}$ is loaded along the upper face of the punch and a frictional constitution with a Coulomb frictional coefficient of $\mu = 0.2$ is used in the HT FE approximation.

Table 3. A range of the number of Trefftz terms

k	1		2		3		...	
t	1	2	1	2	1	2	1	2
m	5	7	9	11	13	15	...	...

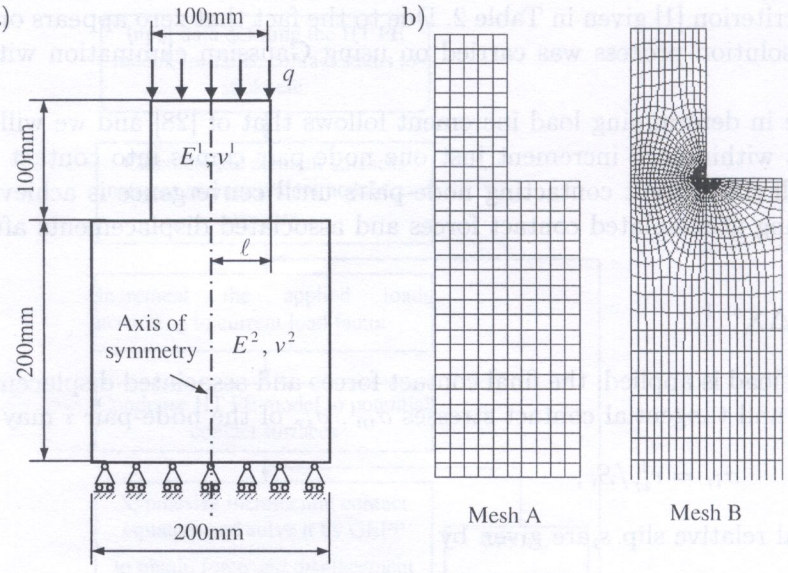

Fig. 6. A punch indented on a foundation

Table 4. Results with various number m of Trefftz terms

Node-pair		1	5	9	13	17	21
X coordinate		0.0	10.0	20.0	30.0	40.0	50.0
$m = 7$	σ_n	1.054976	1.044437	1.044623	1.077558	1.239684	4.355683
	σ_τ	0.000000	0.037462	0.081258	0.152383	0.247937	0.871137
	s_τ	0.000000	0.000000	0.000000	0.000000	0.000438	0.002864
$m = 9, 11, 13, 15$	σ_n	1.058314	1.047577	1.045805	1.074607	1.215687	4.552451
	σ_τ	0.000000	0.036973	0.077333	0.1297468	0.243124	0.910490
	s_τ	0.000000	0.000000	0.000000	0.000000	0.000593	0.003211

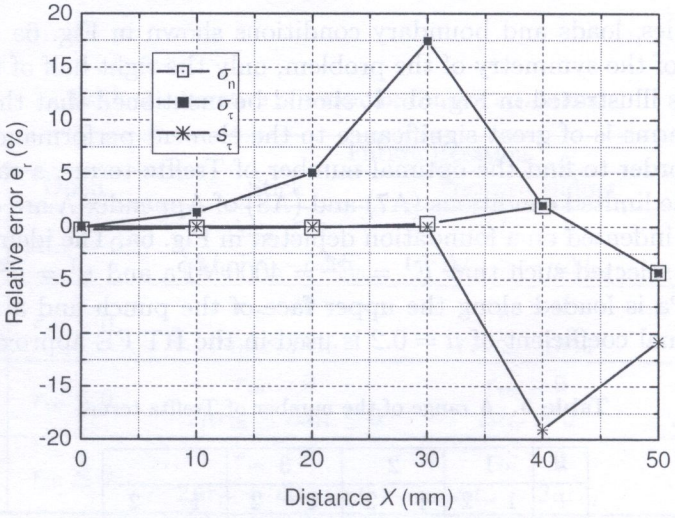

Fig. 7. Relative errors at 5 node-pairs

Mesh A (a coarse mesh) consisting of 250 HT elements and Mesh B (a fine mesh) of 1190 HT elements are used in our analysis. The example is, in fact, a simple contact because its actual length ℓ of contact is known to be 50 mm. The results show that the case of $m = 5$ can give convergent results for Mesh A, but not for Mesh B. This indicates that the minimal number of Trefftz terms may not provide stable results. Table 4 shows the results for a range of m from 7 to 15. It is observed that $m = 9$, 11, 13 and 15 can provide robust and stable results. For clarity, the curve of relative error

$$e_r = 100 \times \frac{f_{m=7} - f_{m=9}}{f_{m=9}} \tag{28}$$

is plotted in Fig. 7. It is observed that $m = 9$ is the optimal number from the point view of either computational time or convergent performance and used in the calculation. As a result, the explicit expression of the 2×9 matrix $\mathbf{N}_e$ in Eq. (3) involving the 9 homogeneous solutions (truncated T-complete functions) and the resultant 3×9 matrix $\mathbf{T}_e$, 2×9 matrix $\mathbf{Q}_e$ are obtained and listed in Appendix B.

Figures 8 and 9 demonstrate the contact stresses and corresponding relative slips on the contact interface with $m = 9$ and a stick zone of a slightly larger that 30 mm is obtained. The results of the HT FEM analysis are compared with those of ABAQUS analysis. It is evident that the results of the HT FEM agree well with those of ABAQUS 6.2.

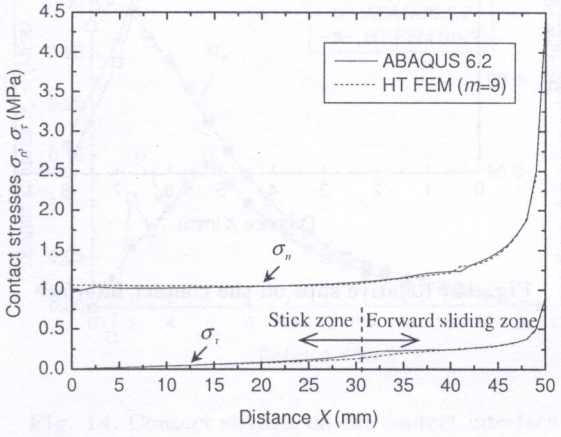

Fig. 8. Contact stresses on the contact interface

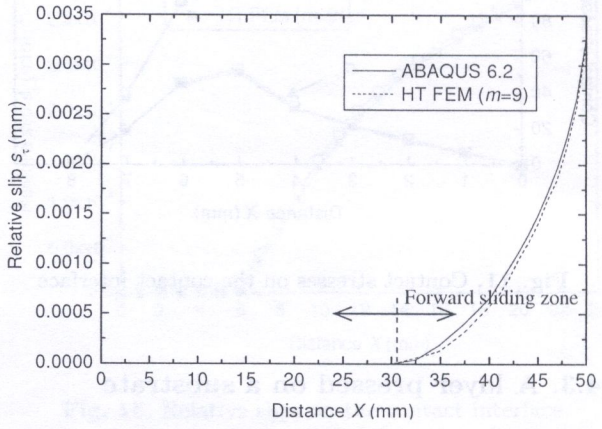

Fig. 9. Relative slips on the contact interface

4.2. An infinite cylinder rest on a rigid semi-infinite medium

The classical Hertz contact of an infinite elastic cylinder on a rigid semi-infinite medium (Fig. 10a), together with geometry and prescribed boundary conditions, is treated here. The same material property as in previous example is used for the sphere and the concentrated force P is 2000 MPa. Coulomb frictional coefficient μ is 0.5. The sphere is discretized in 726 HT elements and the corresponding mesh is shown by Fig. 10b. A potential contact arc of $\ell = 17.189°$ is chosen on each of the surfaces where is distributed with 31 nodes of interval size 0.573°.

Figures 11 and 12 illustrate the distribution of the stresses and relative slips on the contact interface. The hollow square points are ABAQUS 6.2 solutions while the black square points indicate HT FEM results. Again, agreement between ABAQUS 6.2 and HT FEM results is satisfactory.

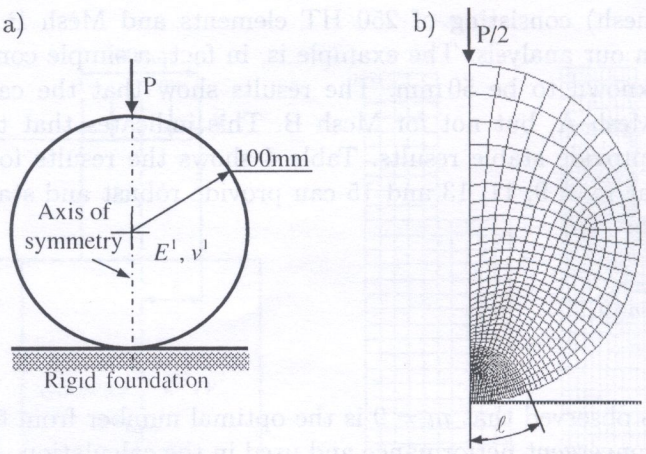

Fig. 10. An infinite cylinder rest on a rigid semi-infinite medium

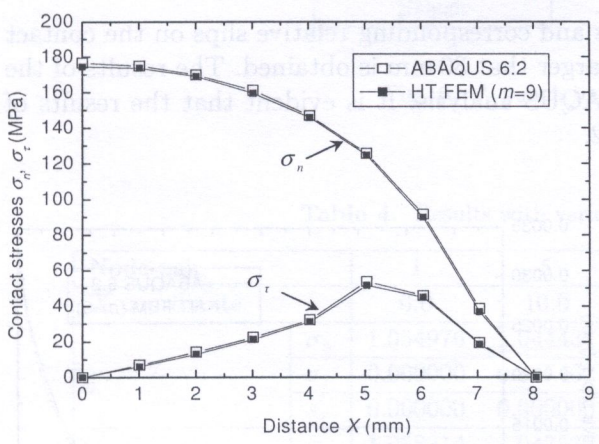

Fig. 11. Contact stresses on the contact interface

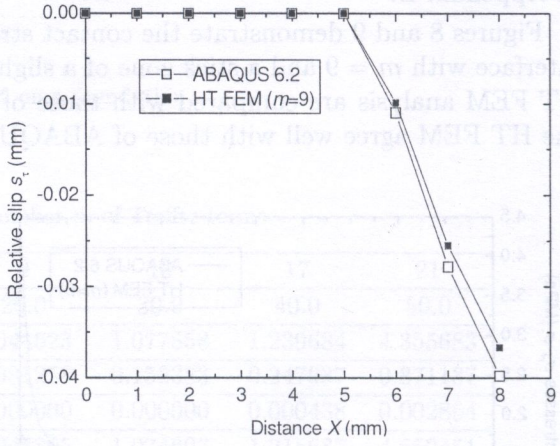

Fig. 12. Relative slips on the contact interface

4.3. A layer pressed on a substrate

Figure 13a shows a classical receding contact problem: a layer pressed on a substrate. The geometrical and prescribed conditions are given in the figure. The problem is discretized with 1040 HT elements (see Fig. 13b). A potential contact length of $\ell = 30\,\text{mm}$ is chosen on both bodies, and contact surfaces on both bodies are defined by 30 equidistant nodes. The concentrated force P is 5 MPa, elastic properties are assumed to be $E^1 = E^2 = 4000\,\text{MPa}$, $\nu^1 = \nu^2 = 0.35$ and Coulomb frictional coefficient μ is 0.8. The results of stress and relative slip distributions are plotted in Figs. 14 and 15. It is observed from Fig. 14 that the ABAQUS 6.2 results are in oscillation at the first 3 node-pairs, and more seriously, the 2nd node-pair has an unacceptable negative tangential stress value of $-0.02916\,\text{MPa}$. In contrast to ABAQUS 6.2 results, the HT FEM ones appear to be stable and reliable. The relative slips predicted by both approaches are close to each other as shown in Fig. 15.

The effect of Young's modulus, Poisson's ratio, Coulomb frictional coefficient and external load on contact behavior can be found from Figs. 16–21. Figure 16 shows the stress distribution on the contact interface for a range of Young's moduli $E^2 = E^1 = 10$, 500, 2000, 4000 and 8000 MPa. The results indicated that the stress distribution does not change with the variation of Young's modulus. This applies both to the frictionless case and the frictional case. However, when the Young's modules of two contact bodies are different, i.e., $(E^2/E^1 \neq 1)$, the contact behavior was significantly affected by the value of Young's modules (Fig. 17). As the substrate becomes more

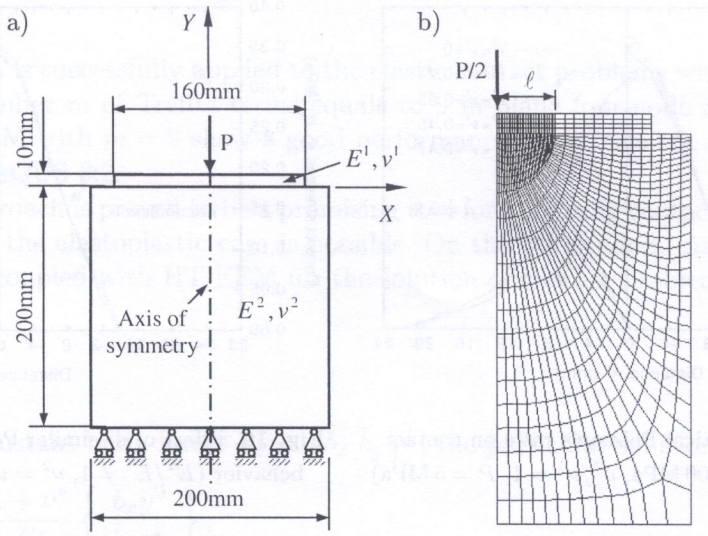

Fig. 13. A layer pressed on a substrate

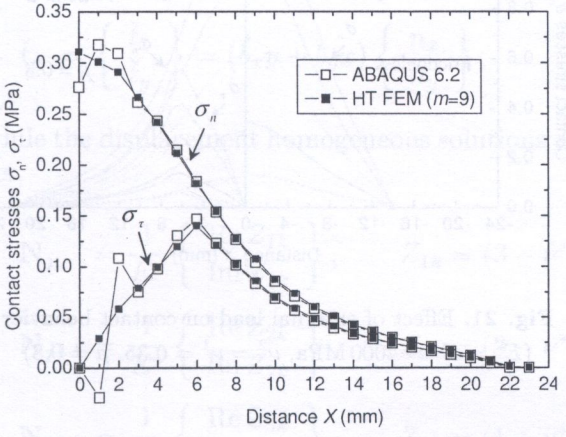

Fig. 14. Contact stresses on the contact interface

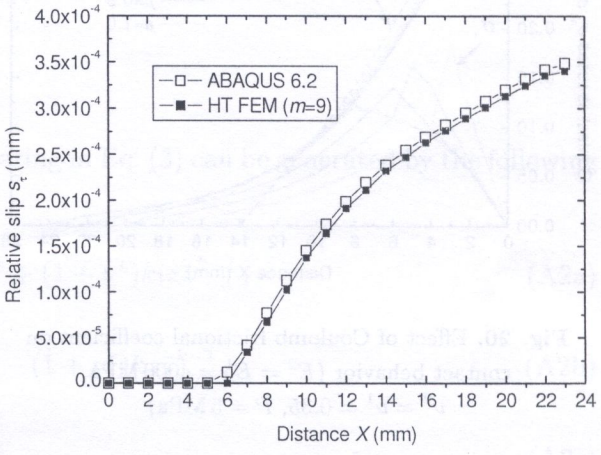

Fig. 15. Relative slips on the contact interface

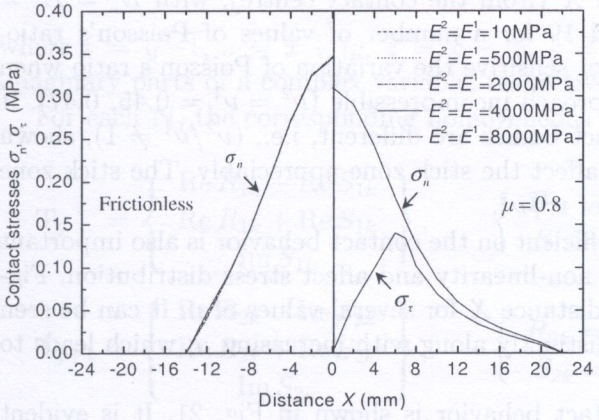

Fig. 16. Effect of identical elastic modulus on contact behavior ($E^2/E^1 = 1$, $\nu^2 = \nu^1 = 0.35$, $P = 5\,\mathrm{MPa}$)

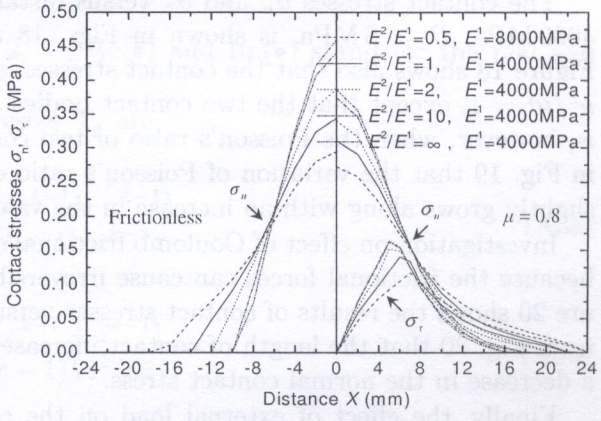

Fig. 17. Effect of dissimilar elastic modulus on contact behavior ($E^2/E^1 \neq 1$, $\nu^2 = \nu^1 = 0.35$, $P = 5\,\mathrm{MPa}$)

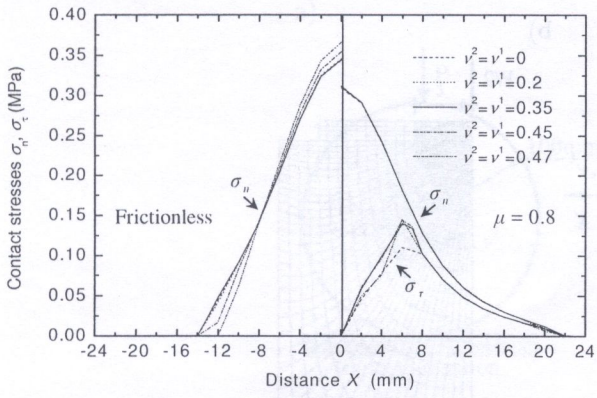

Fig. 18. Effect of identical Poisson's ratio on contact behavior ($E^2 = E^1 = 4000\,\text{MPa}$, $\nu^2/\nu^1 = 1$, $P = 5\,\text{MPa}$)

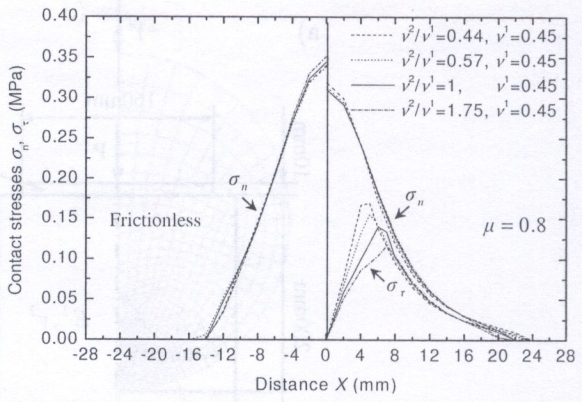

Fig. 19. Effect of dissimilar Poisson's ratio on contact behavior ($E^2/E^1 \neq 1$, $\nu^2 = \nu^1 = 0.35$, $P = 5\,\text{MPa}$)

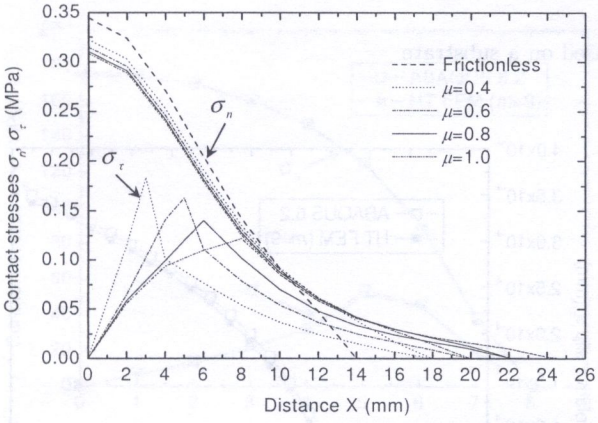

Fig. 20. Effect of Coulomb frictional coefficient on contact behavior ($E^2 = E^1 = 4000\,\text{MPa}$, $\nu^2 = \nu^1 = 0.35$, $P = 5\,\text{MPa}$)

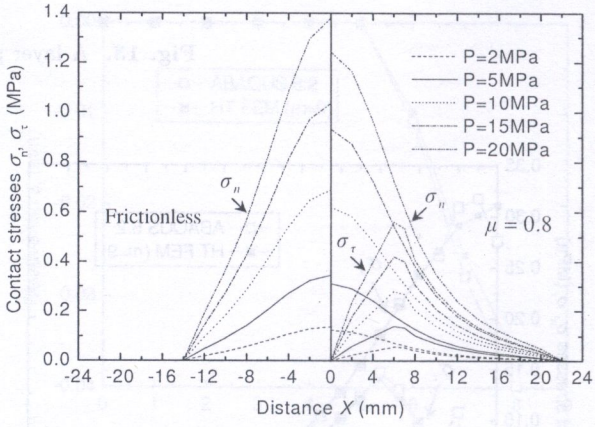

Fig. 21. Effect of external load on contact behavior ($E^2 = E^1 = 4000\,\text{MPa}$, $\nu^2 = \nu^1 = 0.35$, $\mu = 0.8$)

rigid than the layer ($E^2/E^1 > 1$), the normal contact stress at the axis of symmetry increases remarkably, whereas the length of contact decreases. Furthermore, the stick zone reduces slightly in the frictional case.

The contact stresses σ_n and σ_τ versus distance X (from the contact centre), with $E^2 = E^1 = 4000\,\text{MPa}$, $P = 5\,\text{MPa}$, is shown in Figs. 18 and 19 for a number of values of Poisson's ratio. Figure 18 shows also that the contact stresses is not sensitive the variation of Poisson's ratio when $\nu^2/\nu^1 = 1$, except that the two contact bodies approach incompressible ($\nu^2 = \nu^1 = 0.45$, 0.47). It is, however, when the Poisson's ratio of two contact bodies are different, i.e., ($\nu^2/\nu^1 \neq 1$), shown in Fig. 19 that the variation of Poisson's ratio do affect the stick zone appreciably. The stick zone slightly grows along with an increase in the value of ν^2/ν^1.

Investigation on effect of Coulomb frictional coefficient on the contact behavior is also important because the frictional forces can cause irreversible non-linearity and affect stress distribution. Figure 20 shows the results of contact stresses versus distance X for several values of μ. It can be seen from Fig. 20 that the length of contact increases distinctly along with increasing μ, which leads to a decrease in the normal contact stress.

Finally, the effect of external load on the contact behavior is shown in Fig. 21. It is evident that the normal and tangential stresses on the contact interface increase remarkably along with increasing P. it is also observed, interestingly, that the length of contact and the stick zone remain unchanged.

5. Conclusions

The HT FE approach is successfully applied to the elastic contact problems with friction. It is found that the optimal number m of Trefftz terms equals to 9 in plane four-node elements. The results computed by HT FEM with $m = 9$ show a good performance of the element model and agree well with those from ABAQUS 6.2.

The proposed approach is proved to be a promising tool for analyzing contact nonlinear problems. Further extension to the elastoplastic case is possible. On the other hand, mathematical programming technique [24] coupled with HT FEM for the solution of contact problems is underway.

Appendix A

In the presence of constant body forces $\bar{\mathbf{b}}_e = [\,\bar{b}_x\ \bar{b}_y\,]^T$, the particular solutions are given by

$$\begin{aligned}
\breve{\mathbf{u}}_e &= \left\{ \begin{array}{c} \breve{u}_x \\ \breve{u}_y \end{array} \right\} = \frac{1+\nu^*}{E^*} \left\{ \begin{array}{c} \bar{b}_x y^2 \\ \bar{b}_y x^2 \end{array} \right\}, \\
\breve{\boldsymbol{\sigma}}_e &= \left\{ \begin{array}{c} \breve{\sigma}_x \\ \breve{\sigma}_y \\ \breve{\sigma}_{xy} \end{array} \right\} = \left\{ \begin{array}{c} 0 \\ 0 \\ \bar{b}_x y + \bar{b}_y x \end{array} \right\}, \\
\breve{\mathbf{t}}_e &= \left\{ \begin{array}{c} \breve{t}_x \\ \breve{t}_y \end{array} \right\} = (\bar{b}_x y + \bar{b}_y x) \left\{ \begin{array}{c} n_x \\ n_y \end{array} \right\},
\end{aligned} \tag{A1}$$

while the displacement homogeneous solutions appearing in Eq. (3) can be generated by the following set,

$$\mathbf{N}_j = \frac{1}{E^*} \left\{ \begin{array}{c} \mathrm{Re}\, Z_{1k} \\ \mathrm{Im}\, Z_{1k} \end{array} \right\}, \qquad Z_{1k} = (3-\nu^*) i z^k + (1+\nu^*) k i z \bar{z}^{k-1}, \tag{A2a}$$

$$\mathbf{N}_{j+1} = \frac{1}{E^*} \left\{ \begin{array}{c} \mathrm{Re}\, Z_{2k} \\ \mathrm{Im}\, Z_{2k} \end{array} \right\}, \qquad Z_{2k} = (3-\nu^*) z^k - (1+\nu^*) k z \bar{z}^{k-1}, \tag{A2b}$$

$$\mathbf{N}_{j+2} = \frac{1}{E^*} \left\{ \begin{array}{c} \mathrm{Re}\, Z_{3k} \\ \mathrm{Im}\, Z_{3k} \end{array} \right\}, \qquad Z_{3k} = (1+\nu^*) i z^k, \tag{A2c}$$

$$\mathbf{N}_{j+3} = \frac{1}{E^*} \left\{ \begin{array}{c} \mathrm{Re}\, Z_{4k} \\ \mathrm{Im}\, Z_{4k} \end{array} \right\}, \qquad Z_{4k} = -(1+\nu^*) z^k, \tag{A2d}$$

where $i = \sqrt{-1}$, $z = x + iy$, $\bar{z} = x - iy$, $k = 1, 2, \cdots$; $\mathrm{Re}(\bullet)$ and $\mathrm{Im}(\bullet)$ stand for the real and imaginary parts of a complex variable, respectively.

For each $\mathbf{N}_j$,the corresponding homogeneous stresses $\mathbf{T}_j$ are

$$\mathbf{T}_j = \left\{ \begin{array}{c} \mathrm{Re}\, R_{1k} - \mathrm{Re}\, S_{1k} \\ \mathrm{Re}\, R_{1k} + \mathrm{Re}\, S_{1k} \\ \mathrm{Im}\, S_{1k} \end{array} \right\}, \qquad \left\{ \begin{array}{l} R_{1k} = ik(z^{k-1} - \bar{z}^{k-1}) \\ S_{1k} = i(k-1) k z^{k-2} \bar{z} \end{array} \right. \tag{A3a}$$

$$\mathbf{T}_{j+1} = \left\{ \begin{array}{c} \mathrm{Re}\, R_{2k} - \mathrm{Re}\, S_{2k} \\ \mathrm{Re}\, R_{2k} + \mathrm{Re}\, S_{2k} \\ \mathrm{Im}\, S_{2k} \end{array} \right\}, \qquad \left\{ \begin{array}{l} R_{2k} = k(z^{k-1} + \bar{z}^{k-1}) \\ S_{2k} = (k-1) k z^{k-2} \bar{z} \end{array} \right. \tag{A3b}$$

$$\mathbf{T}_{j+2} = \left\{ \begin{array}{c} -\mathrm{Re}\, S_{3k} \\ \mathrm{Re}\, S_{3k} \\ \mathrm{Im}\, S_{3k} \end{array} \right\}, \qquad S_{3k} = k i z^{k-1} \tag{A3c}$$

$$\mathbf{T}_{j+3} = \left\{ \begin{array}{c} -\mathrm{Re}\, S_{4k} \\ \mathrm{Re}\, S_{4k} \\ \mathrm{Im}\, S_{4k} \end{array} \right\}, \qquad S_{4k} = kz^{k-1}. \tag{A3d}$$

Once $\mathbf{T}_j$ have been evaluated, each $\mathbf{Q}_j$ can be given as follows,

$$\mathbf{Q}_j = \left\{ \begin{array}{l} n_x(\mathrm{Re}\, R_{1k} - \mathrm{Re}\, S_{1k}) + n_y \,\mathrm{Im}\, S_{1k} \\ n_y(\mathrm{Re}\, R_{1k} + \mathrm{Re}\, S_{1k}) + n_x \,\mathrm{Im}\, S_{1k} \end{array} \right\}, \tag{A4a}$$

$$\mathbf{Q}_{j+1} = \left\{ \begin{array}{l} n_x(\mathrm{Re}\, R_{2k} - \mathrm{Re}\, S_{2k}) + n_y \,\mathrm{Im}\, S_{2k} \\ n_y(\mathrm{Re}\, R_{2k} + \mathrm{Re}\, S_{2k}) + n_x \,\mathrm{Im}\, S_{2k} \end{array} \right\}, \tag{A4b}$$

$$\mathbf{Q}_{j+2} = \left\{ \begin{array}{l} -n_x \,\mathrm{Re}\, S_{3k} + n_y \,\mathrm{Im}\, S_{3k} \\ n_y \,\mathrm{Re}\, S_{3k} + n_x \,\mathrm{Im}\, S_{3k} \end{array} \right\}, \tag{A4c}$$

$$\mathbf{Q}_{j+3} = \left\{ \begin{array}{l} -n_x \,\mathrm{Re}\, S_{4k} + n_y \,\mathrm{Im}\, S_{4k} \\ n_y \,\mathrm{Re}\, S_{4k} + n_x \,\mathrm{Im}\, S_{4k} \end{array} \right\}. \tag{A4d}$$

In order to make the resulting stiffness matrix have full rank, the choice of the number m of Trefftz terms has to obey a stability condition

$$m \geq NDOF - 3 \tag{A5}$$

as well as a simple 'truncation rule'

$$m = 4k + 2t - 1 \tag{A6}$$

where

$$t = \left\{ \begin{array}{ll} 1 & \text{truncated after (A2b), (A3b) and (A4b),} \\ 2 & \text{truncated after (A2d), (A3d) and (A4d).} \end{array} \right. \tag{A7}$$

APPENDIX B

The homogeneous solutions of $\mathbf{N}_e$, $\mathbf{T}_e$ and $\mathbf{Q}_e$ for $m = 9$ are explicitly expressed by

$$\mathbf{N}_e = \frac{1}{2G} \left[\begin{array}{cccccc} (\kappa{-}1)x & y & -x & -2\kappa xy & (\kappa{-}2)x^2 - (\kappa{+}2)y^2 & \\ (\kappa{-}1)y & x & y & (\kappa{+}2)x^2 - (\kappa{-}2)y^2 & 2\kappa xy & \\ & & & 2xy & y^2 - x^2 & (3{-}3\kappa)x^2y + (\kappa{+}3)y^3 \\ & & & x^2 - y^2 & 2xy & (\kappa{+}3)x^3 - (3\kappa{-}3)xy^2 \end{array} \right. \quad \left. \begin{array}{c} (\kappa{-}3)x^3 - (3\kappa{+}3)xy^2 \\ (3\kappa{+}3)x^2y - (\kappa{-}3)y^3 \end{array} \right], \tag{B1}$$

$$\mathbf{T}_e = \left[\begin{array}{ccccccccc} 2 & 0 & -1 & -6y & 2x & 2y & -2x & -12xy & -12y^2 \\ 2 & 0 & 1 & -2y & 6x & -2y & 2x & -12xy & 12x^2 \\ 0 & 1 & 0 & 2x & -2y & 2x & 2y & 6(x^2+y^2) & 0 \end{array} \right], \tag{B2}$$

$$\mathbf{Q}_e = \left[\begin{array}{ccccccc} 2n_x & n_y & -n_x & 2n_yx - 6n_xy & 2n_xx - 2n_yy & 2n_yx + 2n_xy & 2n_yy - 2n_xx \\ 2n_y & n_x & n_y & 2n_xx - 2n_yy & 6n_yx - 2n_xy & 2n_xx - 2n_yy & 2n_yx + 2n_xy \end{array} \right.$$
$$\left. \begin{array}{cc} 6n_y(x^2+y^2) - 12n_xxy & -12n_xy^2 \\ 6n_x(x^2+y^2) - 12n_yxy & 12n_yx^2 \end{array} \right], \tag{B3}$$

where

$$G = \frac{E^*}{2(1+\nu^*)}, \qquad \kappa = 3 - 4\nu^*. \tag{B4}$$

Acknowledgements

The authors wish to acknowledge the financial support from the Australian Research Council (Grant No. DP0665941).

References

[1] W.J. Chen, X.W. Li. Equivalence between iterative method and nonlinear complementary method for two dimensional contact problems with friction. *Engrg. Mech.*, **18**: 33–38, 2001.

[2] J.A.T. Freitas, Hybrid-Trefftz displacement and stress elements for elastodynamic analysis in the frequency domain. *CAMES*, **4**: 345–368, 1997.

[3] J. Jirousek, L. Guex. The hybrid-Trefftz finite element model and its application to plate bending. *Int. J. Num. Meth. Engrg.*, **23**: 651–693, 1986.

[4] J. Jirousek, N. Leon. A powerful finite element for plate bending. *Comp. Meth. Appl. Mech. Engrg.*, **12**: 77–96, 1977.

[5] J. Jirousek, Q.H. Qin. Application of Hybrid-Trefftz element approach to transient heat conduction analysis. *Comp. Struct.*, **58**: 195–201, 1996.

[6] J. Jirousek, A. Venkatesh. Hybrid Trefftz plane elasticity elements with p-method capabilities. *Int. J. Num. Meth. Engrg.*, **35**: 1443–1472, 1992.

[7] J. Jirousek, A. Venkatesh, A.P. Zieliński, H. Rabemantantsoa. Comparative study of p extensions based on conventional assumed displacement and hybrid-Trefftz FE models. *Comp. Struct.*, **46**: 261–278, 1993.

[8] J. Jirousek, A. Wróblewski. T-elements: State of the art and future trends. *Arch. Comp. Meth. Engrg.*, **3**: 323–434, 1996.

[9] J. Jirousek, A. Wróblewski, B. Szybiński. A new 12 DOF quadrilateral element for analysis of thick and thin plates. *Int. J. Num. Meth. Engrg.*, **38**: 2619–2638, 1995.

[10] S.Y. Ma. The solution of two-dimensional frictionless elastic contact problems using boundary element method. *J. Hebei Instit. Technol.*, **2**: 11–21, 1984.

[11] D. Martín, M.H. Aliabadi. Boundary element analysis of two-dimensional elastoplastic contact problems. *Engrg. Anal. Boundary Elem.*, **21**: 349–360, 1998.

[12] K. Peters, E. Stein, W. Wagner. A new boundary-type finite element for 2-D- and 3-D-elastic structures. *Int. J. Num. Meth. Engrg.*, **37**: 1009–102, 19945

[13] Q.H. Qin. Hybrid Trefftz finite element approach for plate bending on an elastic foundation. *Appl. Math. Modelling*, **18**: 334–339, 1994.

[14] Q.H. Qin. Postbuckling analysis of thin plates by a hybrid Trefftz finite element method. *Comp. Meth. Appl. Mech. Engrg.*, **128**: 123–136, 1995.

[15] Q.H. Qin. Nonlinear analysis of thick plates by HT FE approach. *Comp. Struct.*, **61**: 271–281, 1996.

[16] Q.H. Qin. Transient plate bending analysis by hybrid Trefftz element approach. *Commun. Num. Meth. Engrg.*, **12**: 609–616, 1996.

[17] Q.H. Qin. Postbuckling analysis of thin plates on an elastic foundation by HT FE approach. *Appl. Math. Modelling*, **21**: 547–556, 1997.

[18] Q.H. Qin. Advances in hybrid-Trefftz finite element method. *Adv. Mech.*, **28**: 71–82, 1998.

[19] Q.H. Qin. *The Trefftz Finite and Boundary Element Method.* WIT Press, Southampton, 2000.

[20] Q.H. Qin. Dual variational formulation for Trefftz finite element method of elastic materials. *Mech. Res. Commun.*, **31**: 321–330, 2004.

[21] Q.H. Qin. Trefftz finite element method and its applications. *Appl. Mech. Rev.*, **58**: 316–337, 2005.

[22] Q.H. Qin. Formulation of hybrid Trefftz finite element method for elastoplasticity. *Appl. Math. Modelling*, **29**: 235–252, 2005.

[23] Q.H. Qin, S. Diao. Nonlinear analysis of thick plates on an elastic foundation by HT FE with p-extension capabilities. *Int. J. Solids Struct.*, **33**: 4583–4604, 1996.

[24] Q.H. Qin, X.Q. He. Variational principles, FE and MPT for analysis of non-linear impact-contact problems. *Comp. Meth. Appl. Mech. Engrg.*, **122**: 205–222, 1995.

[25] E. Trefftz. Ein Gegenstück zum Ritz'schen Verfahren. In: *Proc. the 2nd International Congress on Applied Mechanics*, Zurich, Switzerland, 1926; pp. 131–137.

[26] K.Y. Wang, Q.H. Qin, Y.L. Kang, J.S. Wang, C.Y. Qu. A direct constrain-Trefftz FEM for analysing elastic contract problems. *Int. J. Num. Meth. Engrg.*, **63**: 1694–1718, 2005.

[27] E. Wilson. The static condensation algorithm. *Int. J. Num. Meth. Engrg.*, **8**: 199–203, 1974.

[28] J.X. Xu, S.Y. Long. A new load scaling technique for frictional contact problems—Accurate load increment technique used to bring target-pair into contact without causing either under- or over- loading. *J. Hunan Univ.*, **25**: 23–26, 1998.

[29] Y.H. Zhang, M.C. Xi, C.S. Cheng. *Computational Methods and their Algorithms*. Science Press, Beijing, 2000.
[30] A.P. Zieliński. Trefftz method: elastic and elastoplastic problems. *Comp. Meth. Appl. Mech. Engrg.*, **69**: 185–204, 1988.
[31] A.P. Zieliński, O.C. Zienkiewicz. Generalized finite element analysis with T-complete solution functions. *Int. J. Num. Meth. Engrg.*, **21**: 509–528, 1985.